Annu. Rev. Earth Planet. Sci. 1996. 24:89–123

PROBING PLANETARY ATMOSPHERES WITH STELLAR OCCULTATIONS

J. L. Elliot

Department of Earth, Atmospheric, and Planetary Sciences and Department of Physics, Massachusetts Institute of Technology, Cambridge, Massachusetts 02139 and Lowell Observatory, Flagstaff, Arizona 86001

C. B. Olkin

Department of Earth, Atmospheric, and Planetary Sciences, Massachusetts Institute of Technology, Cambridge, Massachusetts 02139 and Lowell Observatory, Flagstaff, Arizona 86001

KEY WORDS: Venus, Mars, Jupiter, Saturn, Titan, Neptune, Triton, Pluto, Charon

ABSTRACT

Earth-based stellar occultations probe the temperature, pressure, and number-density profiles of planetary atmospheres in the microbar range with a vertical resolution of a few kilometers. Depending on the occultation data available for a given body and other information, the technique also allows determination of local density variations, extinction by aerosols and molecules, rotation period and zonal winds, atmospheric composition, and the temporal and spatial variability of an atmosphere. A brief quantitative description of the interaction of starlight with a planetary atmosphere is presented, and observational techniques are discussed. Observational results through 1995 are presented for Venus, Mars, Jupiter, Saturn, Titan, Neptune, Triton, Pluto, and Charon.

INTRODUCTION

Occultations of stars by planetary atmospheres—observed from the vicinity of the Earth—probe the temperature, pressure, and number-density profiles of

0084-6597/96/0515-0089$08.00

planetary atmospheres with a typical vertical resolution of a few kilometers. Because the main process causing the starlight to dim is the spreading of light rays through refraction by the atmosphere of the planet, this method detects all gases in the atmosphere. The technique is sensitive to an altitude interval of about five scale heights at the microbar pressure level, depending on the distance between the observer and occulting planet. For cases when the observer is near the center of the planetary shadow, focusing of the starlight by the occulting planet greatly enhances the stellar flux in the shadow plane and allows much deeper probing of the atmosphere than is possible from the main drop and recovery of the occultation light curve. Results from related techniques not covered by this review include stellar and solar occultations observed from spacecraft near the occulting planet (Smith & Hunten 1990) and occultations of spacecraft radio signals (e.g. Tyler et al 1982). Because of the proximity of the spacecraft to the planet and/or the different wavelengths used (UV and radio), these methods probe altitude ranges of planetary atmospheres different from Earth-based stellar occultations, and somewhat different techniques are used for data analysis.

An earlier review (Elliot 1979) discussed all aspects of stellar occultations for probing bodies in the Solar System and, in particular, covers the atmospheric work done with occultations prior to 1979. A critical test of the method (covered by that review) compared the results of the ϵ Geminorum occultation (Elliot et al 1977a,b; Wasserman et al 1977; Hubbard 1979) with the results from *Viking*, which sent an entry probe into the Martian atmosphere just two months later (Seiff & Kirk 1977). As can be seen in Elliot's (1979) Figure 5, the mean temperature and the characteristics of the gravity waves (Zurek 1974, 1976) determined from the occultation and entry probe agree well within their errors.

Highlights of stellar occultation work on planetary atmospheres since 1979 (and before the spring of 1995, when the literature search for this review was completed) include (*a*) comprehensive probing of the atmospheres of Uranus (Baron et al 1989) and Neptune (Roques et al 1994); (*b*) the first confirmed detection of Pluto's atmosphere (Elliot et al 1989, Hubbard et al 1988a, Millis et al 1993); (*c*) the first occultations observed for Titan (Hubbard et al 1990a, Sicardy et al 1990), Charon (Walker 1980), and Triton (Elliot et al 1994); and (*d*) the first imaging observations of the starlight focused by a planetary atmosphere at the center of its shadow (Nicholson et al 1995).

We begin with a discussion of the occultation process and how the observed stellar flux is related to the physical properties of the occulting atmosphere. Next we describe how the data are recorded and the techniques used for analysis. We then review the new results for each body and end with our conclusions about the main issues in planetary atmospheres that we can hope to address in the future with stellar occultations.

THE STELLAR-OCCULTATION PROCESS

The relation between the stellar flux received by an observer and the properties of the planetary atmosphere through which it passed is not trivial, so here we present the main equations that describe the process. We use the geometric optics approximation for a spherical planet, extending the work of Elliot & Young (1992). As shown in Figure 1, we define a coordinate r that has its origin at the center of the planet and a coordinate y, parallel to r, at a distance D from the planet in the plane of the planet's shadow occupied by the observer. The x-axis, in the plane of Figure 1, lies parallel to the original direction of the starlight and perpendicular to the y-axis. Light from a distant star is incident on a planetary atmosphere from the left, and before it is received by the observer, it interacts with the atmosphere in two ways. The first is refraction—

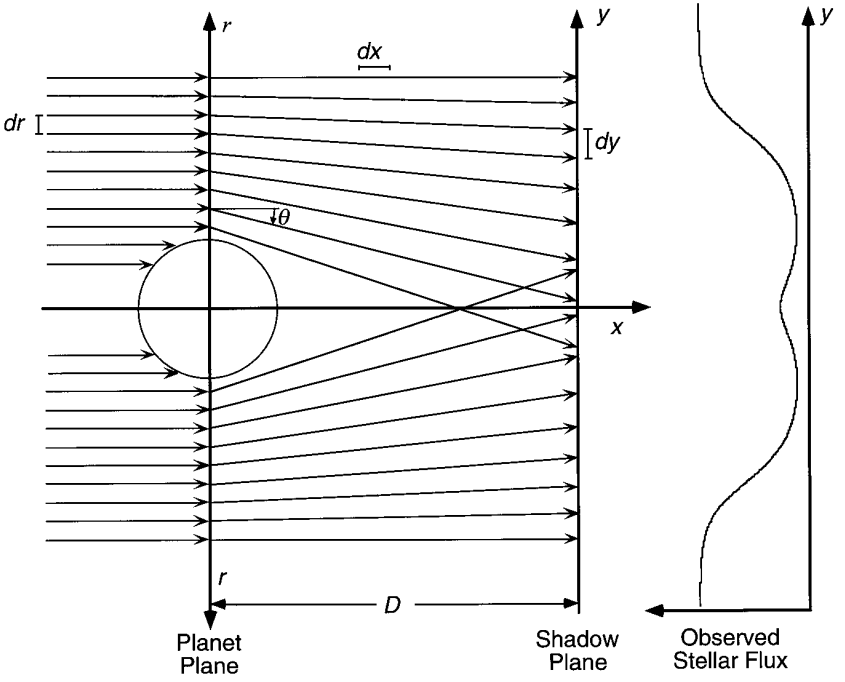

Figure 1 Refraction of starlight by a planetary atmosphere. Starlight incident from the left encounters a planetary atmosphere and is refracted toward the density gradient as illustrated. The exponential gradient causes the rays to spread, which is seen as a dimming of the star by a distant observer located in the shadow plane. In general, light from both the near and far limb contribute to the light curve (depicted at the far right), although the near-limb contribution is dominant.

the most important for Earth-based stellar occultation observations—which spreads the light according to the gradient of the atmospheric refractivity. As shown in Figure 1, refracted light from both the limb nearest to the observer (near limb) and the opposite limb (far limb) can combine at the same location in the shadow. The second effect causing the starlight to dim is extinction, according to the optical depth encountered along the line of sight through the atmosphere. Because the path is tangential, the accumulated optical depth along the path is substantially greater than that for light encountering the atmosphere at normal incidence.

We work with a stellar flux normalized to 1 for the unocculted star. The flux $\zeta(r)$ received by the observer from a single region of the limb of the planet is the product of three factors (Elliot & Young 1992), expressed as a function of the radius r of closet approach of the ray to the center of the planet: 1. $\zeta_s(r)$, a factor that accounts for the refractive spreading normal to the gradient; 2. $\zeta_f(r)$, a factor that accounts for the focusing of the starlight by the atmosphere; and 3. $\zeta_e(r)$, a factor that accounts for the extinction by the planetary atmosphere. Thus

$$\zeta(r) = \zeta_s(r)\zeta_f(r)\zeta_e(r). \tag{1}$$

The spreading factor is simply the absolute value of the ratio of the initial distance between two rays as they encounter the planet, dr, to their distance in the shadow plane, dy. This can be expressed as a function of the refraction angle, $\theta(r)$, experienced by a ray of closest approach r. For refraction toward the center of the occulting body, $\theta(r)$ is defined to be negative (as illustrated in Figure 1). The relation between the refraction angle, shadow-plane coordinate, and radius for closest approach of a ray to the planet's center is $y(r) = r + D\theta(r)$, so

$$\zeta_s(r) = \left|\frac{dr}{dy}\right| = \frac{1}{\left|1 + D\frac{d\theta(r)}{dr}\right|}. \tag{2}$$

The focusing factor is the absolute value of the ratio of the encounter radius to the shadow radius:

$$\zeta_f(r) = \left|\frac{r}{y}\right| = \frac{1}{\left|1 + D\frac{\theta(r)}{r}\right|}. \tag{3}$$

Finally, the extinction factor can be expressed as a function of $\tau_{obs}(r)$, the optical depth encountered by the ray within the planetary atmosphere:

$$\zeta_e(r) = \exp\left[-\tau_{obs}(r)\right]. \tag{4}$$

In order to express the optical depth and refraction angle in terms of fundamental properties of the atmosphere, we introduce a variable of integration, r',

where $r'^2 = r^2 + x^2$, and define $\nu(r')$ to be the refractivity of the planetary atmosphere and $\kappa(r')$ to be its linear absorption coefficient. Then we can write the refraction angle required to a good approximation by Equation 3 as

$$\theta(r) \simeq \int_{-\infty}^{\infty} \frac{r}{r'} \frac{d\nu(r')}{dr'} dx, \tag{5}$$

where the integration is carried out along the path of the ray, which is the x-direction to a good approximation. Similarly, the derivative of the refraction angle is given by

$$\frac{d\theta(r)}{dr} \simeq \int_{-\infty}^{\infty} \frac{x^2}{r'^3} \frac{d\nu(r')}{dr'} + \frac{r^2}{r'^2} \frac{d^2\nu(r')}{dr'^2} dx. \tag{6}$$

The optical depth along the path of the ray is given by a similar integral:

$$\tau_{\rm obs}(r) = \int_{-\infty}^{\infty} \kappa(r') dx. \tag{7}$$

Finally, as illustrated in Figure 1, an observer at a radius $\rho = |y|$ from the center of the shadow will receive a combined stellar flux, $\phi(\rho)$, from two regions of the limb for the spherical planet approximation. Flux from two limbs would also be received outside the "evolute" of the planetary limb, which is the locus of the centers of curvature of the limb, as illustrated in Figure 2 for an elliptical planet (Elliot et al 1977a); inside the evolute (central-flash region), four sections of the planetary limb will contribute to the received flux. For bodies of sufficient angular diameter, the two (or four) contributions to the flux can be resolved and detected separately. If not, the received flux will be the sum from all perpendicular limb points:

$$\phi(\rho) = \sum_{\substack{\text{perpendicular} \\ \text{limb points}}} \zeta(r). \tag{8}$$

To find the stellar flux received by an observer traveling through the occultation shadow, one needs to know the observer's path, $\rho(t)$.

In the geometric optics approximation, the limit on spatial resolution within the atmosphere (in the planet-plane) is set by the finite angular extent of the occulted star—typically about a kilometer, but with many values larger and smaller. For Equation 8 to be a good approximation, the atmospheric scale height should be much larger than both the Fresnel zone (the region of phase coherence for the light; see Born & Wolf 1964) and the diameter of the occulted star projected at the observer-planet distance. If the star has a large angular diameter, one must convolve the result of Equation 8 with the intensity distribution of the star. As one goes deeper into the shadow, the increasing ratio

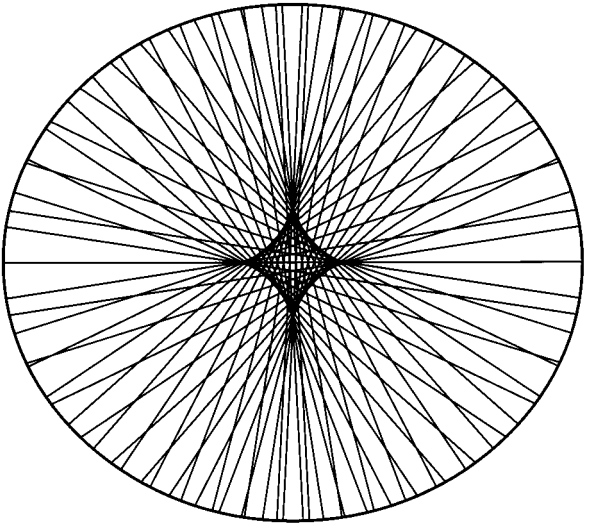

Figure 2 Ray tracing for the central flash. Surfaces of equal bending angle are assumed to be elliptical in shape. Density variations are assumed to be perpendicular to these surfaces, so that light is refracted along the normals to the ellipse. The intersections of these normals form a caustic curve—the evolute of the ellipse. (Adapted from Elliot et al 1977a.)

of the circumference of the planetary limb to that of the shadow causes the stellar diameter to correspond to an ever increasing interval around the planetary limb. Along the path of the light rays, the main contributions to the integrals in Equations 5 and 6 occur over an interval in x of about $(2rH)^{1/2}$ (Elliot & Young 1992), where H is the scale height of the atmosphere at radius r. Consequently, a considerable amount of the atmosphere along the path of each ray contributes to its refraction.

Wave-optical effects become important when the angle subtended by the star is smaller than that subtended by the Fresnel zone—about $(\lambda D)^{1/2}/D$, where λ is the wavelength of the light and D the distance between the observer and occulting body. This value applies to free space, but within the atmosphere the differential phase shifting that causes the decreasing stellar flux improves the angular resolution in the direction of the phase gradient (the radial direction) to $\phi(\lambda D)^{1/2}/D$. Wave-optical theory as it applies near the center of the shadow (the central-flash region) has been derived by Hubbard (1977).

For turbulent atmospheres, one needs a statistical treatment for the intensity fluctuations in the shadow pattern. This theory has been developed analytically by Narayan & Hubbard (1988) and numerically by French & Lovelace (1983), following the earlier work of Young (1976).

OBSERVATIONAL METHODS

In this section we briefly discuss the acquisition of stellar-occultation data and the calibrations essential for subsequent analysis. The object of the observations is to reconstruct the occultation pattern formed in the shadow plane (discussed in the previous section). A rigorous reconstruction is impossible with present techniques, since it would require an imaging detector as large as the shadow of the occulting body! The measurement we can obtain, however, is the stellar intensity along the observer's path within the shadow versus time (called a "light curve"), but the large-scale symmetry of most bodies allows us to reconstruct the shadow pattern from just a few of these light curves. The starlight seen by the observer is affected by the atmosphere above the perpendicular limb points. For a central path, these do not change with position within the shadow, while for any other paths (sometimes called "chords"), these points are a function of position within the shadow, with the greatest change occurring for the least central events.

In selecting occultations suitable for observation, one keeps in mind a set of scientific objectives, for these dictate the signal-to-noise ratio (S/N) that will be required. For atmospheric work, the S/N per scale height that can be achieved with a given telescope and photometer is a good indicator of data quality. In estimating the S/N, the background light from the occulting planet is the limiting factor for most events, but in some cases background from twilight or the Moon can be significant. Observations from more than one station usually enhance what can be learned from an occultation. Portable telescopes allow one to select the location of the chords observed in the shadow plane, with NASA's Kuiper Airborne Observatory (KAO) allowing particularly large changes on short notice.

Predictions of which stars will be occulted have been exhaustively investigated and published for some bodies (Dunham et al 1991, McDonald & Elliot 1995), while for others, this information (likely not complete) is circulated informally within the community. For smaller bodies (whose shadow paths are much narrower than the Earth), refinement of the predicted path is critical, and great efforts are expended in astrometric observations to refine the prediction (Olkin & Elliot 1994).

The detectors used for occultation observations include photomultipliers, IR single-pixel detectors, optical arrays, and IR arrays. Array data are becoming more popular, since they can be modeled to remove the planetary background more effectively than with a conventional photometer, and smaller effective apertures can be used, taking in less background (and its associated noise) along with the stellar image. Array data also allow separation of near-limb and far-limb images, if the planet can be resolved, and they can be used for astrometric

calibrations of the path of the planet with respect to the star. However, array data require the extra step of making the light curve from photometry of each frame, and much more data must be recorded (an entire frame or portion of a frame, rather than a single number) for the same time resolution.

In selecting filters, one usually prefers the large throughput of a broadband filter (or just the bare detector) to achieve the greatest S/N with respect to photon noise. However, the well-defined mean wavelengths provided by narrower filters are necessary for certain applications, such as "spike-delay" analyses (to be described later) and learning the extinction of the planetary atmosphere as a function of wavelength (for those cases when extinction can be measured). Observations can be carried out at multiple wavelengths simultaneously, or even as spectra. By taking the ratio of light curves recorded for different wavelengths, one can remove the effects of variable backgrounds and variable transparency if the background and the star have different colors (Elliot et al 1975b). For planets with deep methane bands, great gains in blocking the planetary background can be achieved by observing through a methane filter, but one may not want the extinction of the starlight that occurs when the starlight probes deeper into the planetary atmosphere (Nicholson et al 1995).

For an observer moving with velocity v in the plane of the shadow, the time taken to cross the "main beam" of the Fresnel diffraction pattern is about $(\lambda D)^{1/2}/v$. To record the highest frequencies in the occultation light curve, one should use an integration time that is half of this interval, although such high-speed recording is not necessary to capture most of the information in the data. The integrations should be contiguous, with no "dead time" between them. Radio time signals from WWV were formally used as a time calibration standard (needed to accurately relate the positions of chords in the shadow plane recorded by different observers), but more recently the Global Positioning System (GPS) has come into widespread use for this purpose. The GPS has an added advantage of providing accurate spatial coordinates of the observer; this is particularly critical for portable and moving observatories, such as the KAO.

In addition to recording the occultation itself, one must also make calibration observations to accurately remove the planetary and other sources of background. Array data need flat-field, dark, and bias calibrations as well. Finally, ground-based observers are at the mercy of atmospheric conditions, and some published occultation data have been recorded under conditions that would have shut down other photometrists. One must be cautious in the interpretation of the data recorded under less than ideal conditions—caution, unfortunately, has not always been heeded.

ATMOSPHERIC INFORMATION FROM OCCULTATION DATA

Learning about planetary atmospheres from stellar occultation light curves first requires a geometric reconstruction of the path of the observer through the shadow plane (Figure 3). This is most usually done by modeling an elliptical planetary figure (at a common level of light-curve flux) from several chords of known relative positions (Millis et al 1993), but this task can also be carried out from accurate astrometric measurements of the star and occulting body (Olkin et al 1996). Once the shadow-plane path has been established, the first-order information that one can extract about the atmosphere is its scale height—even if one does not know its composition. However if the composition is known, and one is willing to make certain assumptions, then temperature, pressure, and number-density profiles can be derived. Local variations in number density due to atmospheric waves and/or turbulence, which cause "spikes" in the occultation light curves, can also be characterized (spikes are large, abrupt increases in the stellar flux, followed by an abrupt return to normal; see Figure 4). If significant extinction affects the light curves, then multiple-wavelength observations can constrain the size of the aerosols. From stellar-occultation probes at multiple latitudes, the ellipticity of an atmosphere can be determined and zonal-wind

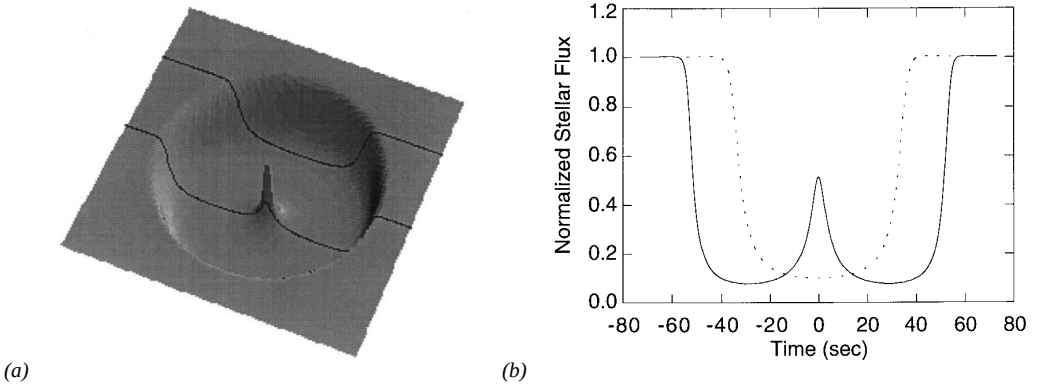

(a) *(b)*

Figure 3 The occultation shadow, with light curves for two different observers. (*a*) A three-dimensional view of the occultation shadow; the vertical dimension is the starlight intensity. Paths of two observers through the shadow pattern are indicated—one passing close to the center and another passing further away. Near the center of the shadow, the starlight is concentrated, due to focusing by the planetary atmosphere, causing the light curve for an observer passing near the center to exhibit a central flash, as can be seen in panel (*b*).

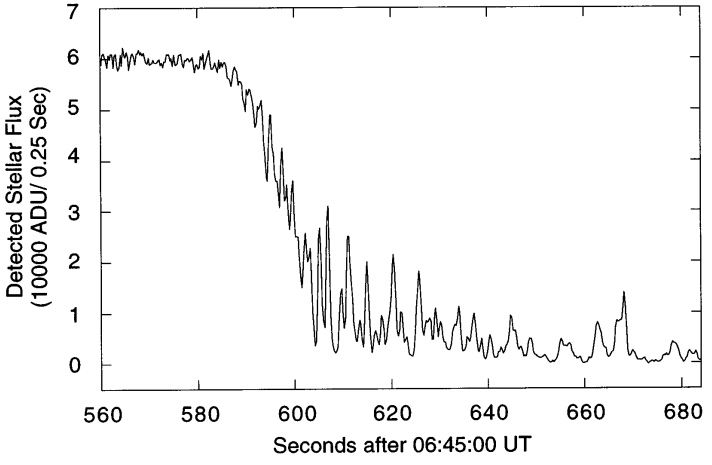

Figure 4 Light curve from an occultation by Saturn's atmosphere. The immersion (disappearance) of 28 Sgr behind the atmosphere of Saturn causes the main drop in the stellar signal. The sharp increases in intensity ("spikes"; most numerous in these data between 600 and 620 s) are caused by small density changes in Saturn's atmosphere, due either to turbulence or wave phenomena. (From unpublished data of J Harrington, ML Cooke, WJ Forrest, JL Pipher, EW Dunham, and JL Elliot.)

profiles inferred. For certain cases, information about the composition of an atmosphere can also be revealed through the time delay of spikes in dual-wavelength observations.

Scale Height

In the first published discussion (known to us) of how a planetary atmosphere affects starlight during an occultation, Pannekoek (1904) demonstrated that the scale height of the atmosphere and the apparent motion of the planet relative to the star control the rate of dimming. Later, Baum & Code (1953) derived a model light curve for an isothermal atmosphere in hydrostatic equilibrium, and they compared their model (calculated for different scale heights) to an occultation light curve they recorded for Jupiter. The scale heights derived depend critically on knowledge of the background level. Hubbard et al (1972) found that a 10% error in background subtraction can lead to a 100% error in the scale height derived from an isothermal fit.

The isothermal model was extended to small planets with thermal gradients and haze by Elliot & Young (1992). Because the scale height derived from fitting this type of model is strictly a number-density scale height, one must allow for the possibility of thermal gradients when deriving a temperature. For

data of high S/N, a possible thermal gradient can be discerned (Elliot & Young 1992).

Once the scale height H has been extracted from the light curve (usually by fitting a model), we can find the ratio of the temperature T to its mean molecular weight μ using the gas constant R and the local gravity g at the occultation level:

$$T/\mu = gH/R. \tag{9}$$

Hence, one must know the mean molecular weight in order to learn the temperature. We call the "temperature" determined in this manner the "equivalent isothermal temperature" (for further explanation, see Elliot & Young 1992). The error in the scale height and other light-curve parameters expected from data with a given S/N is given in Appendix B of French et al (1978). Model fitting is regularly used to determine the mean scale height for first-order analyses (French et al 1983, Hubbard et al 1995, Roques et al 1994). An example of model fitting to the Pluto light curve obtained in 1988 (Elliot et al 1989) is shown in Figure 5. "Immersion" refers to the section of the light curve corresponding to the star first disappearing behind the planet, while "emersion" refers to the reappearance.

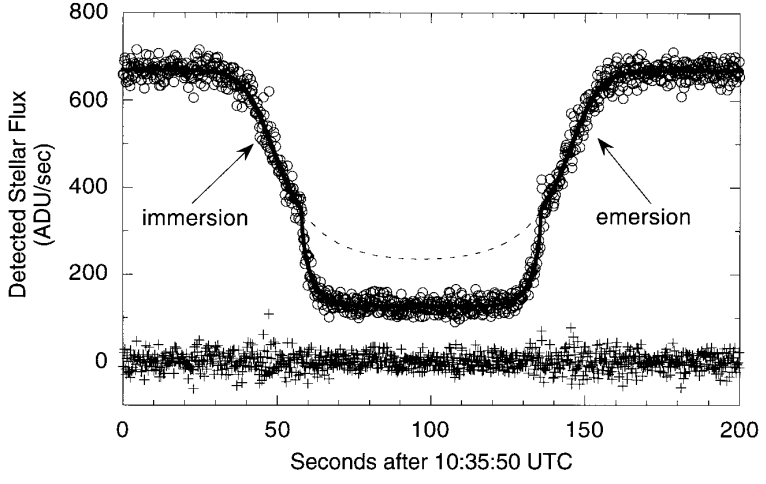

Figure 5 Pluto occultation light curve from the KAO. The gradual decrease in the starlight is caused by Pluto's atmosphere—if there were no atmosphere, the light curve would drop abruptly, in the manner of a Fresnel diffraction pattern. Just below half intensity, the starlight drops more abruptly, indicating either an extinction layer or sharp thermal gradient in Pluto's atmosphere. An isothermal-temperature model that fits the upper atmosphere is indicated by the dashed line. The solid-line model includes extinction, and the residuals from this fitted model are shown along the bottom. (From Elliot & Young 1992.)

Temperature, Pressure, and Number-Density Profiles

For nonisothermal atmospheres, the standard method for determining their thermal structure is the numerical inversion of Equations 2 and 6, which has been treated by several authors (Kovalevsky & Link 1969, Wasserman & Veverka 1973b, Vapillon et al 1973, French et al 1978). The recovered refractivity profile as a function of altitude can be converted to number density if one knows the molecular composition of the atmosphere, and then pressure and temperature profiles can also be derived if one assumes hydrostatic equilibrium. In using the inversion technique one assumes that the refractivity of the atmosphere is a function of radius only and that atmospheric refraction is the only mechanism responsible for the dimming of the stellar flux (although in principle one could add extinction if one had a rule for relating the amount of extinction to the refractivity, or equivalently, the number density). Additional assumptions inherent in the numerical inversion method and the errors expected from photon noise are given by French et al (1978).

The great advantage of numerical inversion is that it does not require one to know the form of the temperature dependence with altitude. With it, one can derive whatever form of the temperature (or pressure or number-density) profile the light curve dictates. However, it does require accurate initial conditions to construct an accurate profile in the upper pressure levels probed. Figure 6 (from Roques et al 1994) demonstrates the sensitivity of numerical inversions to initial conditions. Note that as one goes deeper into the atmosphere, the systematic error introduced by erroneous initial conditions decreases. Another critical factor in retrieving accurate results from numerical inversion is knowledge of the correct background subtraction to define the zero level of the stellar flux in the occultation light curve. An incorrect background affects the temperature profiles, mostly at the lowest altitudes.

Local Density Variations

Local variations in the density are manifested by spikes in occultation light curves (see Figure 4). There has been much discussion over the cause of these variations; in particular, are they due to random turbulence or coherent waves in the planet's atmosphere? Evidence suggests that both mechanisms play a role. Spikes in both the Martian and Jovian atmosphere have been interpreted as scintillations due to isotropic turbulence (Jokipii & Hubbard 1977, Hubbard 1979), while those same spikes in the Martian atmosphere have also been interpreted as waves (Elliot et al 1977a, French & Elliot 1979). Analysis of the August 15, 1980 occultation by Uranus demonstrated that the spikes in three Chilean light curves are not due to turbulence (unless it is extremely anisotropic), because the same light-curve features are present in light curves recorded from

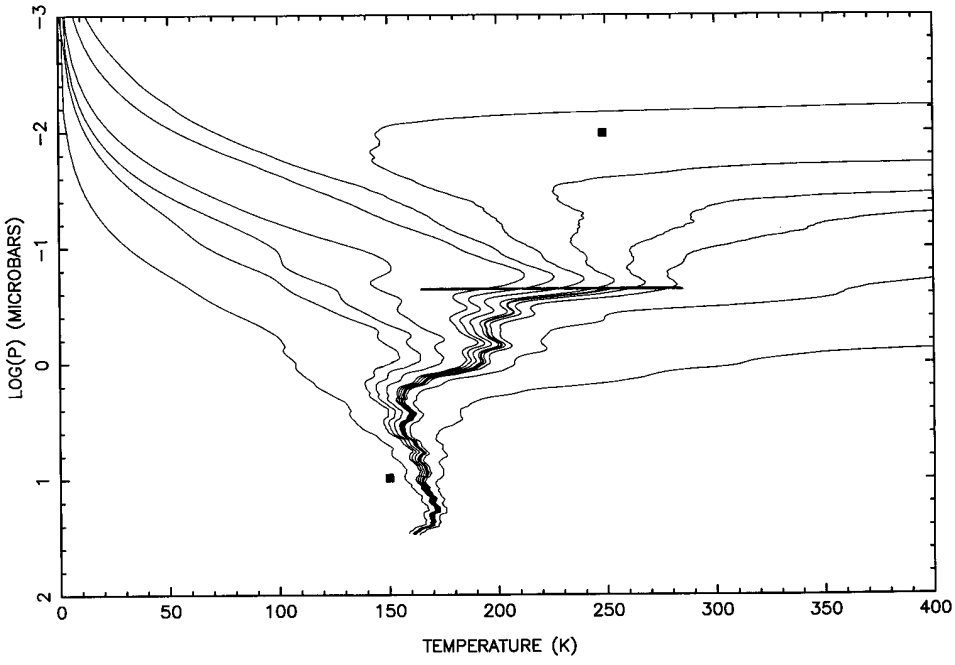

Figure 6 Effects of initial conditions on light curve inversions. The field of solutions of the inversion method applied to the European Southern Observatory August 20, 1985 immersion data, where the large differences at low pressures depend on the initial conditions used to begin the inversion. The squares are the temperatures derived from the *Voyager 2* UVS occultations, and the thicker temperature profile is the preferred solution. (From Roques et al 1994.)

stations over 100 km apart (see Figure 7). The features are consistent with coherent, low-amplitude ($\pm$ 5 K) temperature variations with a vertical scale of several kilometers (French et al 1982). Although the physical mechanisms causing light-curve spikes have not yet been unequivocally determined, French et al (1983) have shown that the numerical inversions are "only weakly influenced by a horizontally inhomogeneous atmospheric structure." Therefore, the temperature profiles derived from the numerical inversions are still valid in the presence of spikes.

Extinction by Aerosols and Molecules

Although differential refraction is the main mechanism causing the starlight to dim for Earth-based observations of a stellar occultation, effects of extinction and/or molecular absorption have been noted deeper in certain atmospheres (in the central-flash portions of the light curves). Separating the effects of

extinction and differential refraction can be aided with simultaneous observations at two or more wavelengths, but it usually requires more information than in the occultation data itself (such as an independent determination of either the extinction or the thermal structure). Two properties of aerosol particles can be characterized by stellar occultations: (*a*) their linear absorption coefficient and (*b*) their size. The linear absorption coefficient can be deduced from the observed optical depth. The aerosol particle size can be constrained from multiple wavelength observations, preferably from the same station.

Extinction by aerosols has been detected in Titan occultation data (Hubbard et al 1993b) and possibly for Pluto as well (Elliot & Young 1992). Effects of molecular absorption have been noted for Saturn (Nicholson et al 1995) and possibly for Neptune (Lellouch et al 1986).

Rotation Period and Zonal Winds

For a rotating body in hydrostatic equilibrium, the body's oblateness, rotation period, and gravitational harmonics are related by a single equation (Brouwer & Clemence 1961). Thus if two of these quantities are known, one can find the third. The oblateness of a body at the half-light level of an occultation (or on an

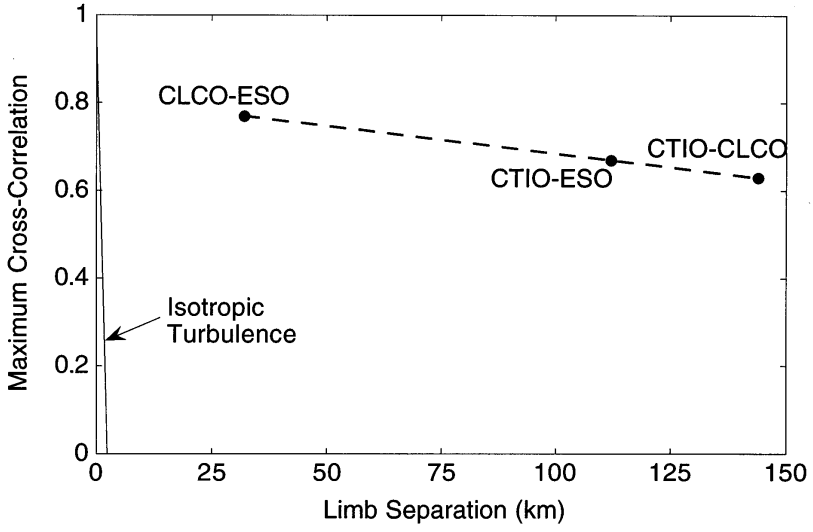

Figure 7 Cross-correlation of light-curve residuals as a function of separation distance along the limb of Uranus. The correlation remains high for observing sites separated by 150 km, decreasing slowly with distance. The correlation extends much further than predicted on the basis of isotropic turbulence theory (Jokipii & Hubbard 1977) and provides evidence that the atmosphere is strongly stratified. (From French et al 1982.)

isobaric surface) can be established with multiple occultation chords (French et al 1985). Another approach for establishing the oblateness is through the structure of the central flash (Elliot et al 1977a, Hubbard et al 1993b, Nicholson et al 1995), from which one can determine the figure at the central-flash level. Early atmospheric occultation data were used to determine the oblateness of Uranus and (along with the gravitational harmonics determined from the ring precessions) to estimate the rotation period prior to the *Voyager 2* encounter (Elliot et al 1980).

With accurate values for all three quantities—oblateness, rotation period, and gravitational harmonics (from a spacecraft encounter or from a kinematic model of ring precessions)—deviations from hydrostatic equilibrium caused by zonal winds can be established. This method has been used to investigate zonal winds for Saturn (Nicholson et al 1995), Titan (Hubbard et al 1993b), and Uranus (Baron et al 1989).

Composition

Brinkmann (1971) was the first to note that occultation light curves with sharp spikes could be used to determine the mixing ratio of a two-component atmosphere, if the refractivities of the two components exhibit different dependencies on wavelength. For an occultation observed at multiple wavelengths (from a single site) there is a time delay between spikes seen in the different wavelength light curves. The time delay is related to the ratio of the atmosphere's refractivity at the two different wavelengths. Once the refractivity dependence on wavelength is known, the contribution due to each of the principal components can be determined. Elliot et al (1974) improved upon the methods of Wasserman & Veverka (1973a) and Brinkmann (1971) and applied this analysis to the emersion light curve of the β Sco AB occultation by Jupiter (the immersion light curve was not as high quality). For Jupiter, the resulting helium fraction by number was found to be $0.16^{+0.19}_{-0.16}$ (Elliot et al 1974); this is consistent with the solar abundance of 0.18 ± 0.04 determined from a combined analysis of *Voyager* data (Conrath et al 1984). This method was also applied to the ϵ Gem occultation by Mars in 1976, and the argon fraction was found to be $0.10^{+0.20}_{-0.10}$ (Elliot et al 1977a). This result is consistent with the later *Viking* result of 0.016 (Owen et al 1977).

Compositional information can also be learned from molecular absorption (Lellouch et al 1986), as described earlier.

Temporal and Spatial Variability of Atmospheres

Ground-based stellar occultation observations provide a relatively inexpensive method (compared to spacecraft) for regular probes of planetary atmospheres. Understanding the time variability of the atmospheric structure of a planet

should aid our understanding of seasonal and climatic changes, especially for those bodies that have large predicted seasonal variations such as Pluto and Triton (Spencer & Moore 1992, Hansen & Paige 1992, Stern & Trafton 1984). Uranus may also exhibit detectable seasonal variations in the structure of its upper atmosphere, since its polar axis is highly inclined to its orbit plane. Observations of an occultation by multiple observing stations can probe different latitudes on the planet (French & Elliot 1979, Baron et al 1989, Roques et al 1994, Hubbard et al 1995).

Comparisons with Other Techniques

Several other techniques can be used to establish the structure of planetary atmospheres near the pressure levels probed by Earth-based stellar occultations: atmospheric entry probes, occultations of radio signals from spacecraft, solar occultations, and stellar occultations observed from spacecraft. It is useful to put the information from stellar occultations in perspective with that from other techniques used for the same purpose. For discussion purposes we choose Neptune as an example, because all these techniques (except for an atmospheric entry probe) have been applied to it. Much of what we know about the structure of Neptune's atmosphere comes from the 1989 encounter by the *Voyager 2* spacecraft. The imaging data were used to study the clouds and cloud motions (Smith et al 1989), but well above the clouds, three instruments onboard were sensitive to the atmospheric structure: (*a*) the infrared interferometer spectrometer (IRIS; Conrath et al 1989), (*b*) the ultraviolet spectrometer (UVS; Broadfoot et al 1989), and (*c*) the radio science subsystem (RSS; Tyler et al 1989). The results of these are displayed in Figure 8 (except for the IRIS observations, which are sensitive to temperatures much deeper in the atmosphere: 30–1000 mbar).

The UVS instrument (Broadfoot et al 1989) recorded solar spectra (between 0.05 and 0.17 μm) as Neptune occulted the Sun. Different mechanisms are responsible for the dimming of the star at different wavelengths. For example, the dimming in the wavelength range of 0.1570 to 0.1634 μm is due to opacity from Rayleigh scattering in H_2. This establishes the temperature of 150 K in the 1 to 100 μbar pressure range (where stellar occultations are also sensitive). The temperature above this region (at 10^{-2} μbar) is determined to be 250 K from H_2-band data (Broadfoot et al 1989). The immersion and emersion temperature profiles from the RSS are shown in Figure 8 (Tyler et al 1989). The temperature profiles from numerical inversion of a stellar occultation observed less than two months before the spacecraft encounter are also indicated in Figure 8, as is the temperature from a central flash observation in 1985 (Roques et al 1994). The central-flash data probe almost as deeply as the RSS data.

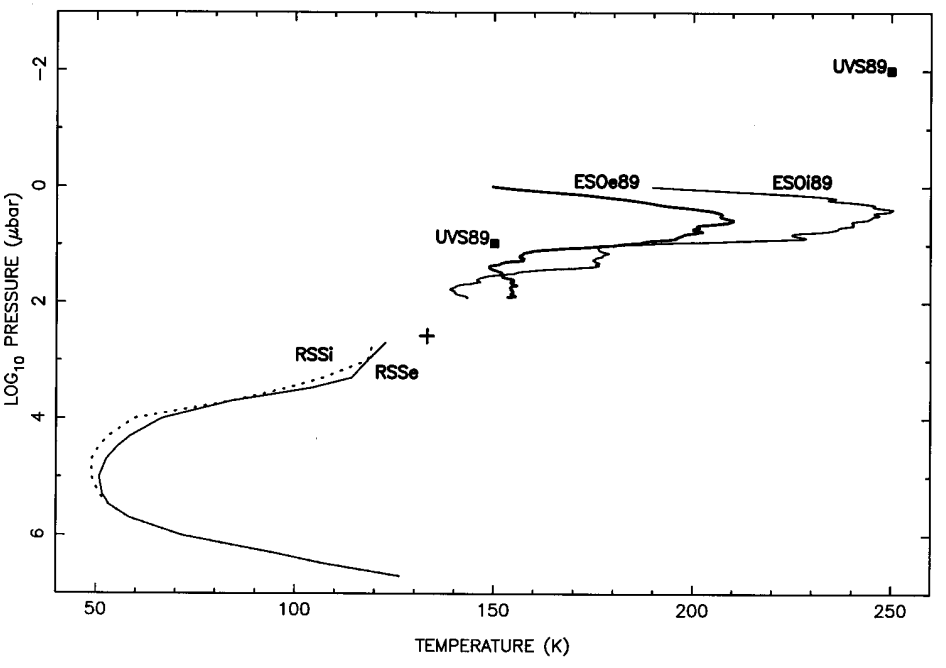

Figure 8 Thermal profile of Neptune's upper atmosphere: comparison of stellar occultation results with the *Voyager 2* results. Temperature profiles for the July 7, 1989 occultation observed at the European Southern Observatory are shown. The temperature derived by Hubbard et al (1987), from the central flash of August 20, 1985 observed in Chile, is indicated by a cross. Two temperature profiles from the radio science observations are indicated. The dotted line is the immersion profile (RSSi); the solid line is the emersion profile (RSSe). The squares are the temperatures derived from the *Voyager 2* ultraviolet spectrometer (UVS). (From Roques et al 1994.)

RESULTS FOR INDIVIDUAL BODIES

In this section we discuss results for individual bodies in their order from the Sun. Table 1 gives a summary of occultation probes of planetary atmospheres, including the major results for each body. Figure 9 illustrates the levels in the atmosphere that can be probed by Earth-based stellar occultation observations. These regions depend on the distance between the observer and occulting body, which changes by a significant factor for Mars and Venus.

Venus

One stellar occultation by Venus has been observed, and that was of the bright star Regulus in 1957. Although there were a plethora of visual observations

(Taylor 1963), the only photoelectric observations were made under difficult conditions in daylight (deVaucouleurs & Menzel 1960). After an attempt to reconcile these results with models based on spacecraft measurements of the Venusian atmosphere, Veverka & Wasserman (1974) concluded that "there is no way in which the Regulus occultation light curve can be reconciled with reality." More information is given in the previous review (Elliot 1979). Unfortunately, to learn about the Venusian atmosphere with stellar occultations we must await a future opportunity, for which data taken with modern array detectors should prove more reliable.

Table 1 Stellar occultation probes of planetary atmospheres

Body	Year(s) observed	Number of probes[a]	Synthesis references[b]	Main results
Venus	1957	2	Veverka & Wasserman (1974)	Data inadequate for firm conclusions
Mars	1976	16	French & Elliot (1979), French & Taylor (1981), Texas-Arizona Occultation Group (1977)	Temperature profiles showing gravity waves, extinction from central flash, oblateness
Jupiter	1952, 1971, 1989	11	Hunten & Veverka (1976), Hubbard et al (1995)	Temperature profiles for different latitudes
Saturn	1989	2	Nicholson et al (1995)	Zonal winds
Titan	1989, 1995	25	Hubbard et al (1993b); HB Hammel, JL Elliot, CB Olkin, unpublished data	Temperature profiles, aerosol size, aerosol N-S asymmetry, zonal wind profile
Uranus	1977, 1979, 1980, 1981, 1982, 1983	23	Baron et al (1989)	Temperature[c] vs latitude and time, oblateness
Neptune	1968, 1983, 1985, 1986, 1987, 1988, 1989, 1990	32	Roques et al (1994), French et al (1985)	Temperature profiles vs latitude and time, oblateness
Triton	1993, 1995	14	JL Elliot, CB Olkin, EW Dunham, unpublished data	Temperature[c]
Pluto	1988	13	Millis et al (1993)	Temperature[c], lower atmospheric structure (haze?, thermal gradient?)
Charon	1980	2	Elliot & Young (1991)	Upper limit on an atmosphere (possibly, an atmosphere was detected)

[a]"Probe" refers to an immersion or emersion section of a light curve or to a single central flash (multiwavelength observations counted only once); the number is the total number of useful probes given in the synthesis papers.
[b]The reference may synthesize just one aspect of the data set(s), such as the temperature profiles or oblateness measurements.
[c]Equivalent isothermal temperature (see text).

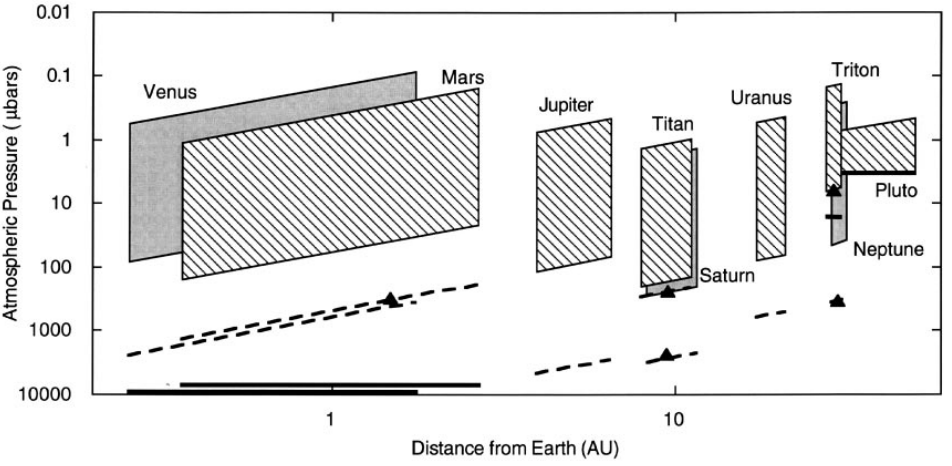

Figure 9 Levels probed by stellar occultations observed from Earth. The main drop and recovery of a stellar-occultation light-curve probe about five scale heights in altitude, with a placement that depends on the refractivity of the planetary atmosphere and the distance between the observer and occulting planet. Planets whose distance goes through large changes offer opportunities for probing different altitude ranges. The Saturn and Titan regions have been slightly offset horizontally for visibility. For Pluto the region is cut off by the surface (as indicated by horizontal line). The surface of Mars and the cloud tops of Venus are also indicated by horizontal lines. The deeper levels probed by central-flash observations are indicated by the dashed lines. A central flash has been observed for five planetary atmospheres, as indicated by the triangles.

Mars

The occultation of ϵ Geminorum by Mars in 1976 occurred just weeks prior to the *Viking* entry probe and at the height of a debate on whether the spikes in stellar-occultation light curves represented the signatures of random atmospheric turbulence (Young 1976) or that of coherent, wave-like atmospheric structures (Elliot & Veverka 1976). It also marked the first observations of a central flash (Elliot et al 1976, 1977a). For the most part, the wave hypothesis seemed the correct explanation for spikes in the Martian occultation light curves (Elliot et al 1977a,b; French & Elliot 1979), as the wave structures derived from inversion of the light curve matched the atmospheric tides observed with the *Viking* entry probe in wavelength and amplitude (Seiff & Kirk 1977, Elliot 1979). Hubbard (1979), however, presents a dissenting view. French & Taylor (1981) used the observations of the April 8, 1976 occultation by Mars to determine an oblateness for the atmosphere and then related that to a mean equator-to-pole temperature difference of more than 50 K. Elliot (1979) gives a more complete discussion of the observations and analyses.

Jupiter

Of the three observed occultations by Jupiter, the first two (occurring in 1952 and 1971) were covered previously (Elliot 1979), so we concentrate here on the last one, observed from one site in 1989 (Hubbard et al 1995). Improvements in instrumentation (in particular the advent of IR array detectors) prior to this event permitted good quality data to be acquired, even though the occulted star (SAO 78505) is much fainter than stars previously occulted (σ Ari and β Sco).

Hubbard et al (1995) fit a Baum & Code (1953) model to get the average scale height and found agreement with results from the β Sco event, which was widely observed in 1971. These results are shown in Figure 10. Numerical inversions of the light curve yielded temperature profiles for Jupiter's mesosphere. These proved reliable only down to the 10 μbar region, due to uncertainties in the background calibration. Even though the *Voyager* instruments are not sensitive to this pressure region, data from the UVS and RSS instruments would put the mean temperature at 220 K—which is above the mean temperature from this occultation, 176 ± 12 K (Hubbard et al 1995). Future probes of this region by

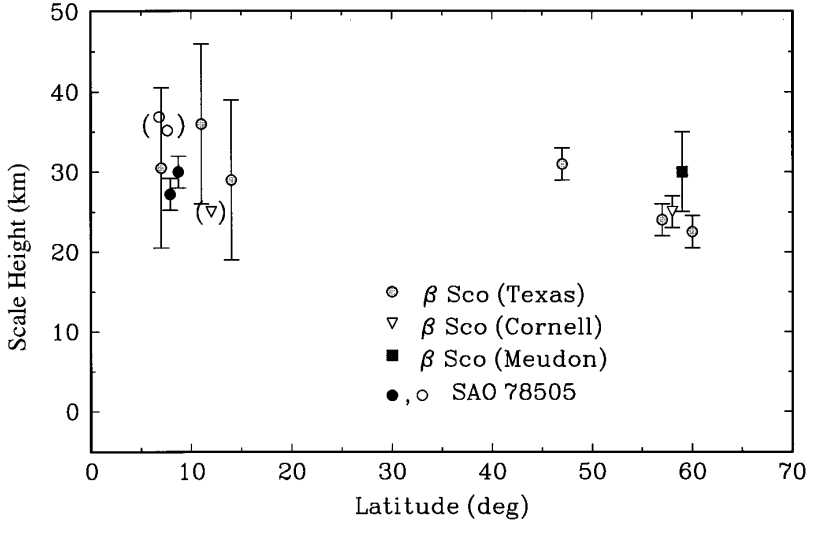

Figure 10 Determination of scale heights in the Jovian mesosphere versus latitude. The β Sco observations were published as follows: Texas group (Hubbard et al 1972), Cornell group (Veverka et al 1974, Elliot et al 1975a), Meudon group (Combes et al 1971). The Cornell data point for β Sco C shown in parentheses was considered highly uncertain, and no error bar was given (Hunten & Veverka 1976). Solid dots and open dots are results from Hubbard et al (1995), for different apertures used to reduce their array data; the other data are from the 1971 β Sco occultation. (From Hubbard et al 1995.)

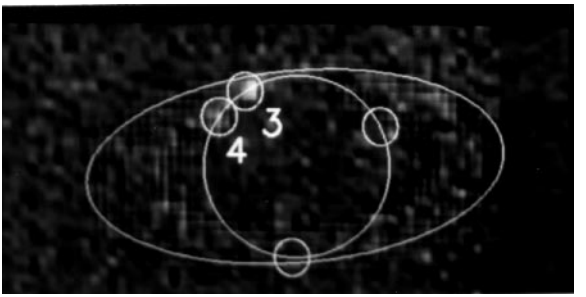

Figure 11 Images of a Saturn central flash for the 28-Sgr occultation, as recorded from McDonald Observatory. This figure is a composite of sixty 0.2-sec integrations taken through a 2.1 μm filter while the observer was within the evolute of Saturn's shadow. The circles show the four positions of the stellar images of the central flash, but only #3 and #4 are bright enough to be seen (on the southwestern limb). Outlines of the limb of Saturn and the outer edge of the A Ring have been added to the frame for reference. (From Nicholson et al 1995.)

ground-based stellar occultation observations and the *Galileo* probe are needed to improve our understanding of the temperature in Jupiter's mesosphere.

Saturn

Our information about Saturn's atmosphere from stellar occultations comes from the 28-Sgr event that occurred on July 3, 1989 and was widely observed throughout the western hemisphere. Although much work has been published on analyses of the ring occultations (French et al 1993, Harrington et al 1993, Hubbard et al 1993a, Elliot et al 1993), the only results (other than abstracts) published to date concerning the atmosphere have been observations of the central flash and their analysis to determine Saturn's stratospheric zonal winds at the 2.5-mbar pressure level (Nicholson et al 1995). These are the first imaging observations of the central flash and were carried out at 2.1 μm from McDonald Observatory and at 3.9 μm from Palomar. These wavelengths have relatively weak CH_4 absorption, which allowed the good transmission at the central-flash level, compared with observations at 2.33 μm (Hubbard et al 1993a), where no central flash could be detected. Another aspect of the observations is that Saturn's rings were open, causing significant interference with the central flash observations (Nicholson et al 1995).

The data were recorded as a time series of images, from which a light curve was constructed. However, within the evolute (Elliot et al 1977a), images of the star from four different regions of the planetary limb are visible; samples of these are shown in Figure 11 (Nicholson et al 1995). An individual light curve for each of the flash images was generated and compared with a model.

Nicholson et al (1995) found that the data are most sensitive to the zonal wind profile (since this accounts for the difference of the global limb shape from hydrostatic equilibrium), with the best agreement for a uniform wind speed of 40 m s^{-1} at 25–70° north latitude in the stratosphere. Comparison with zonal wind profiles determined by *Voyager* at the cloud level suggests that the mid-latitude winds decay with height above the troposphere to the nonzero mean of local tropospheric winds (Nicholson et al 1995).

Two puzzling discrepancies remain between the data and the model used by Nicholson et al (1995). The first is a relative offset of 3 s between the times of the McDonald and Palomar data: This is much larger than the 0.05 s limit established from the ring-orbit modeling (French et al 1993). The second is that the observed central-flash profiles are substantially smoother than the model profiles, even if one accounts for the larger angular diameter subtended by the star. A similar effect occurs for Mars, where the central flash is smoother than the model (Elliot et al 1977a). One explanation of this effect for Saturn offered by Nicholson et al (1995) is that refractive scintillations (Narayan & Hubbard 1988, Hubbard et al 1988b), produced by wave structure or turbulence in Saturn's atmosphere, could be responsible.

Numerous immersion and emersion light curves were recorded for the 28-Sgr occultation (see Figure 4 for one example), and analysis of 14 of these should appear in the literature soon (WB Hubbard, private communication).

Titan

To date only two ground-based stellar occultations by Titan have been observed (Sicardy et al 1990; Hubbard et al 1990a; HB Hammel, JL Elliot & CB Olkin, unpublished data). However, the first event significantly increased our knowledge of Titan's atmospheric structure in the 250–450 km altitude range because of three factors: 1. the brightness of the occulted star (28 Sgr), 2. the almost 50% coverage of the occultation shadow, and 3. light curves that were recorded over a large range of wavelengths. The event was observed from 15 stations, with 6 stations recording the central flash. The wavelengths of the observations ranged from 0.39 μm to 0.89 μm (Hubbard et al 1993b). Although the *Voyager* spacecraft had already visited Titan by the time of this occultation, it did not probe the atmosphere at the same altitude. The UVS stellar occultation probed Titan at altitudes above 1000 km (Smith et al 1982), whereas the RSS data were sensitive to higher pressure levels, in the altitude range of 0–200 km (Lindal et al 1983).

Results of inverting the occultation light curves show that the stratospheric temperature on Titan is between 150 and 170 K, with no temperature differences between the sunset and sunrise limb and no temperature differences between the equatorial and high southern latitudes (Hubbard et al 1993b).

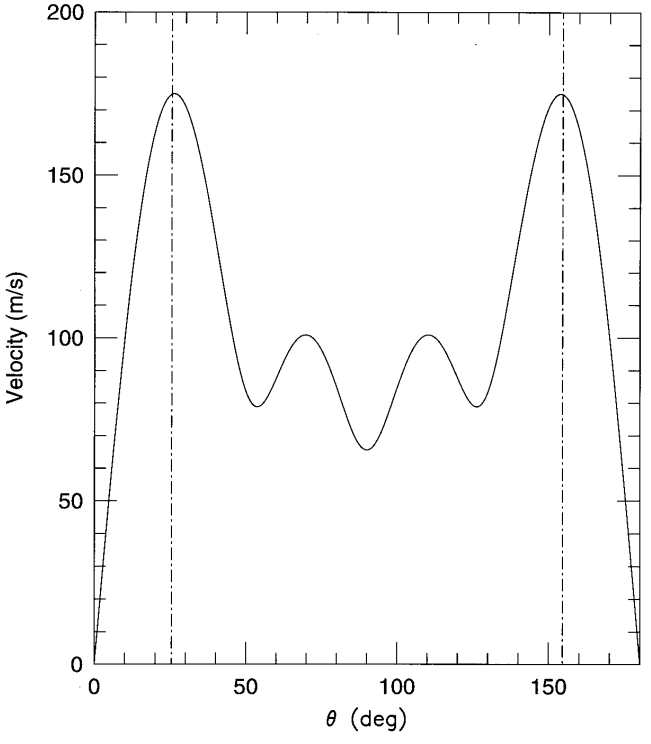

Figure 12 Titan zonal winds. Zonal flow in Titan's stratosphere, as a function of colatitude θ, inferred from the best-fit differentially rotating model for the 28-Sgr occultation. Vertical dashed lines delimit the range of θ near the pole, where no occultation data are available because of the tilt of Titan's spin axis to the reference plane. (From Hubbard et al 1993b.)

The central flash from the 1989 occultation by Titan has been used to determine the limb shape, from which a zonal wind profile was derived by Hubbard et al (1993b). They noted that the central-flash pattern observed by the six most-central stations in the Titan occultation of 28 Sgr was not consistent with the evolute pattern expected by a oblate planet (Elliot et al 1977a) and proposed a differentially rotating model for Titan's stratosphere. The resulting zonal flow velocity is shown in Figure 12.

In contrast to the consistent stratospheric temperatures derived, latitudinal asymmetries in the aerosol distribution are evident. Asymmetries in the baseline of three light curves and the suppression of central-flash caustics from the north limb of Titan indicate the presence of two haze regimes: (*a*) a high-optical-

depth haze over Titan's north pole and equatorial regions and (*b*) a relatively low-optical-depth haze over the south pole (Hubbard et al 1993b).

Imaging observations (from both *Voyager* and *HST*) have detected hemispheric albedo asymmetries. However, the *Voyager* observations show the opposite asymmetry, with the detached, higher-optical-depth haze layer in the south pole and equatorial regions (Toon et al 1992). More recent *HST* observations (Caldwell et al 1992) showed the northern hemisphere of Titan to be brighter than the south (consistent with the asymmetric hazes found from the 1989 stellar occultation). This asymmetry has been attributed to large-scale Hadley circulation (Toon et al 1992) associated with Titan's seasonal cycle.

Uranus

Many stellar occultations by Uranus were observed in order to improve kinematic models for the Uranian rings (Elliot et al 1981, French et al 1986) prior to the *Voyager 2* encounter in 1986. Baron et al (1989) present a synthesis of all the occultation data from 1977 to 1983 to derive an oblateness of 0.0197 ± 0.0010 for the Uranian atmosphere at the μbar pressure level. [The accuracy is comparable to the determination of the figure at the 1 bar level by *Voyager 2* radio occultations (Lindal et al 1987).] The rotation period inferred from the oblateness, 17.7 ± 0.6 h, is consistent with the 17.24 h period derived from periodic radio signals caused by the magnetic field rotation (Warwick et al 1986).

Twenty-three determinations of the average atmospheric temperature are also included in the analysis of Baron et al (1989). As can be seen in Figure 13, these temperatures show no obvious change with latitude. However, over the seven-year time span of the observations the temperature appears to increase at the rate of 8 K/year (Figure 13). The cause of the apparent increase of temperature with time is not known, although we note that the increase depends heavily on the 1977 observations.

Neptune

A large number of Neptune occultations have been observed, mostly as by-products of the search for rings (Elliot et al 1985, Hubbard et al 1986). A combined analysis of 22 light curves from 9 stellar occultations observed during the period 1983–1990 has been presented by Roques et al (1994). They analyze the data by fitting isothermal models to the light curves and by numerical inversions. Preferring the results from the inversions, they find mean temperatures in the range 150–200 K at the 25-μbar pressure level. As discussed earlier, this level lies between the *Voyager* UVS and RSS measurements (see Figure 8), and their results confirm the general increase in temperature from the tropopause to the lower thermosphere. The inversions show 30-K variations of temperature occurring over 30-km altitude ranges (the scale height is about

50 km). Roques et al found no observed correlation between latitude and temperature, but did report a possible correlation between the mean temperature from numerical inversions and the 11-year solar cycle. More data are required to confirm this correlation, however. Possible signatures of extinction by hazes were noted in some of the light curves.

Roques et al (1994) analyzed eight central flash events from these light curves. They used an isothermal analysis to find scale heights from 28 to 48 km in the pressure range from 300 to 400 μbars (81 K to 138 K; no error bars are given, but much of this range must be due to errors rather than temperature differences in Neptune's atmosphere). Hubbard et al (1988b) examined the scintillations in one of the central flash events, and a Monte Carlo simulation of Neptune's shadow is shown in Figure 14. The central flash observed in 1985 was analyzed by Lellouch et al (1986), under the assumption that deviations from the stratospheric temperature are due to absorption by CH_4, from which they infer that $[CH_4]/[H_2] = 0.6\%$ (with an uncertainty of a factor of 10) at 0.3 mbar. Hubbard et al (1987) prefer to interpret the central-flash data in terms of a thermal gradient, and they find that the temperature changes from 150 to 135 K as the pressure rises from 1 to 400 μbar.

Triton

The inferred variability of Triton's surface pressure with season (Hansen & Paige 1992, Spencer & Moore 1992) makes this an interesting target for a series of occultation observations. Some models predict extremely large changes in surface pressure (several orders of magnitude), while other models predict less.

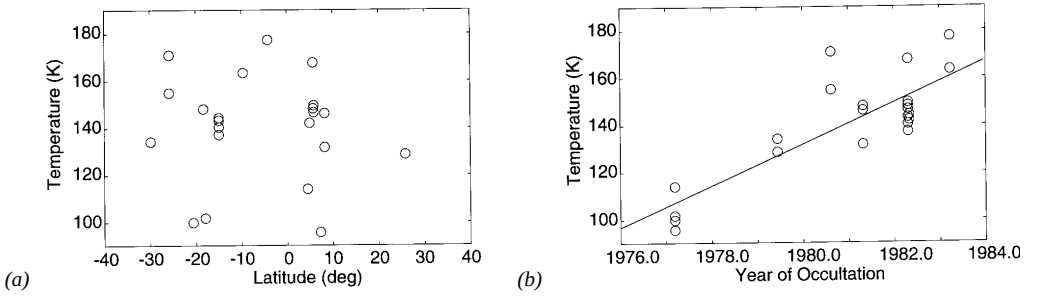

Figure 13 (*a*) Mean Uranian atmospheric temperature near the 1-μbar pressure level as a function latitude. In spite of the greater insolation experienced in high northern latitudes, there is no systematic trend in temperature with latitude. (*b*) Mean Uranian atmospheric temperature near the 1-μbar pressure level, plotted against the observation date. In spite of the range of latitudes covered by the observations, there persists a systematic increase in temperature with date. The straight line, intended merely to be suggestive, corresponds to an upper atmospheric heating rate of about 8 K/year. (From Baron et al 1989.)

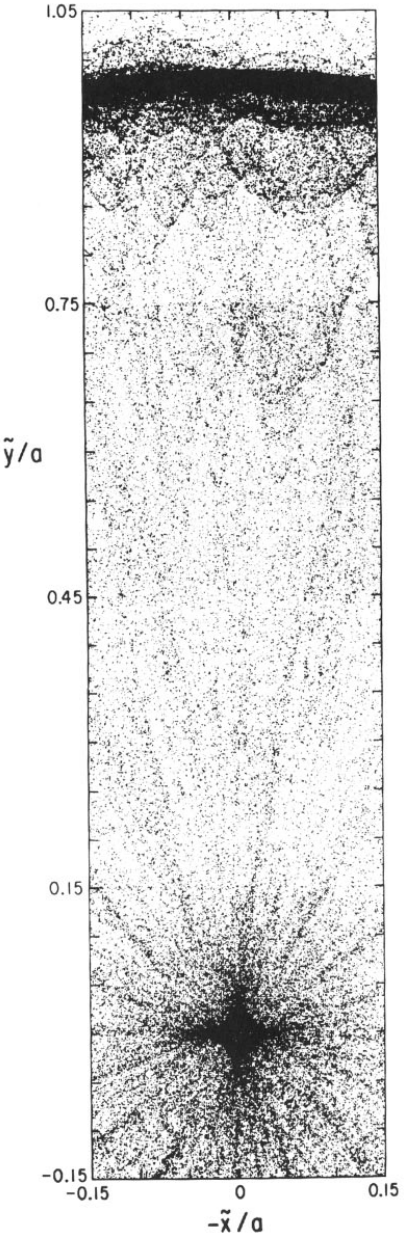

Figure 14 Montage of Monte Carlo simulations in various regions of Neptune's occultation shadow. In this figure, direct rays that are not appreciably deflected by the atmosphere are cut off so that the scattered component above the limb is visible. (From Hubbard et al 1988b.)

The state of Triton's atmosphere was approximately determined in 1989 by several instruments aboard *Voyager 2*. Each of these instruments investigated a different region of the atmosphere and was sensitive to different properties. Aeolian features noted on images of the surface have been used to define the pattern of surface winds, while the remarkable "plumes" (Smith et al 1989) trace wind speeds up to an altitude 8 km, where the troposphere ends. The radio occultation found a high electron density at 400-km altitude (implying the presence of an ionizing heat source) and detected the neutral atmosphere near the surface (Tyler et al 1989). The UVS measurements of spectra and occultations were in the range 500–1700 Å (Broadfoot et al 1989, Yelle et al 1991). From the spectral data, N_2 and NII were detected, and from the *Voyager 2* occultation data, strict limits were placed on the amount of CO. The [CO]/[N_2] ratio is less than one percent, so Triton's atmosphere is almost purely N_2.

To investigate possible changes in the surface pressure, KAO observations of a stellar occultation were carried out in 1993 (Elliot et al 1994). An isothermal model based on the work in Elliot & Young (1992) was fit to the occultation light curve, with haze consistent with the *Voyager 2* imaging observations (Hillier & Veverka 1994) included in the model. Results for the temperature and number density show that Triton's atmosphere exhibited no detectable change since the *Voyager 2* encounter (JL Elliot, CB Olkin, EW Dunham, unpublished data). A second Triton occultation was widely observed in August 1995 (see Table 1), but results are not yet available.

Pluto

Attempts to observe a stellar occultation by Pluto date back to 1965 (Halliday 1965), but the first definitive observations of a stellar occultation occurred in 1988. This occultation was recorded by seven ground stations in New Zealand and Australia (Millis et al 1993), but the KAO provided the light curve with the best S/N (Elliot et al 1989). These data are displayed in Figure 5, where the points represent 0.2-s integrations and the lines represent models discussed below. The gradual drop of the light curve from the unocculted stellar signal is caused by Pluto's atmosphere. In the upper part of the light curve there may be one or two spikes, but the scarcity of these relative to giant-planet occultation light curves indicates that Pluto's atmosphere is much more stable (fewer waves and/or turbulence) than the giant-planet atmospheres. The dashed line in Figure 5 shows a model isothermal atmosphere. The light curve follows the isothermal model until about half intensity, and then it abruptly drops well below the isothermal model, which can be explained in two ways: Either (*a*) Pluto's atmosphere has a haze layer with a sharp upper boundary (Elliot et al 1989, Elliot & Young 1992) whose extinction causes the light curve to abruptly drop or (*b*) Pluto's atmosphere has a thermal gradient (Eshleman

1989, Hubbard et al 1990b) strong enough ($\sim$ 20 K/km) to accomplish the same effect.

If we concentrate on the analysis of the upper, isothermal part of the light curve for the moment, Elliot & Young (1992) find T/μ for this part of the atmosphere to be 3.72 ± 0.75 (K/amu) and find a thermal gradient consistent with zero. Surface-ice spectroscopy by Owen et al (1993) revealed N_2, CO, and CH_4, from which these authors concluded that the predominant constituent is N_2, because it has by far the highest vapor pressure at the 40 ± 2 K temperature of Pluto's surface (Tryka et al 1994).

The structure of Pluto's atmosphere as determined from the 1988 occultation is shown in Figure 15, where we have indicated the uncertainty in the lower part of the atmospheric structure that can be due to the extinction or sharp thermal gradient. This ambiguity could be resolved with future occultation observations, carried out simultaneously in the IR and visible. Haze particles would be small and produce less extinction at IR wavelengths so that the light curve would not drop so steeply as the optical. On the other hand, if the sharp drop is due to a thermal gradient, then the IR and optical light curves would appear virtually identical.

The model that describes the isothermal character of the upper part of the light curve, as established from the analysis of Elliot & Young (1992), was put forth by Yelle & Lunine (1989). Due to the large cross sections of CH_4, it absorbs sunlight in the 3.3-μm band and then reradiates in the 7.7-μm band, keeping the temperature at a nearly constant 102 K. Lellouch (1994) pointed out that CO cooling could be significant in the radiative transfer, and Strobel et al (1995) have incorporated CO cooling into a more sophisticated model. However, these radiative transfer models have not yet demonstrated that they can generate temperature changes that are abrupt enough to explain the sharp drop in the light curve (Figure 5). Similarly, the haze interpretation of the sharp drop in the light curve suffers from no known mechanism to produce enough particles and to keep them suspended (Stansberry et al 1994).

Millis et al (1993) find a remarkable consistency among the temperatures of the isothermal part of the atmosphere and the radius of the "top of the haze" around the planet. Also, the surface radius deduced by them (1195 ± 5 km for the sharp-thermal-gradient assumption) is about 30–40 km larger than that deduced from the mutual events (Buie et al 1992, Young & Binzel 1994). One explanation for this is that a deep troposphere could hide the surface from the occultation light curves, except for the more central stations (Stansberry et al 1994).

Some models predict that Pluto's atmosphere will collapse as it recedes from the Sun, but this conclusion depends on the CH_4 fraction in Pluto's volatile reservoir (Trafton 1990). JA Stansberry (private communication) points out

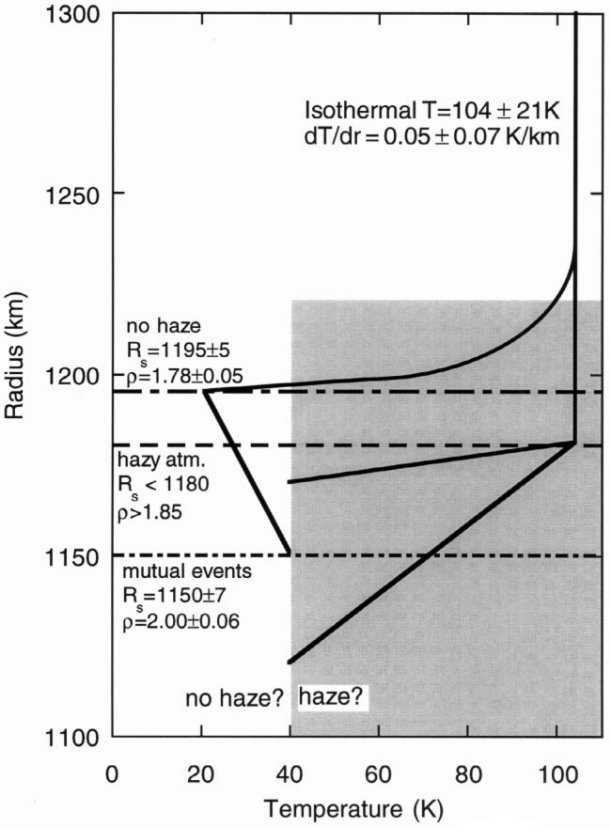

Figure 15 Structure of Pluto's atmosphere. The upper atmosphere is consistent with an isothermal temperature profile, while there are different possibilities for the lower atmosphere. A clear lower atmosphere requires a sharp thermal gradient, and the observed surface radius from Millis et al (1993) of 1195 ± 5 km is consistent with the surface radius from the mutual events (Buie et al 1992) if a troposphere underlies the sharp thermal gradient (Stansberry et al 1994) as depicted in the figure. The drop in the occultation light curve can also be explained by extinction and a thermal gradient (which may be more gradual). Two such profiles are shown. (Adapted from Elliot & Young 1992.)

that the alpha-beta phase transition for N_2 could buffer the atmosphere at the transition temperature (35.6 K) and keep it from collapsing for part of its orbit.

Charon

A stellar occultation of a 12th magnitude star by Charon was observed by Walker (1980), who used these data to set a lower limit on Charon's radius of 600 km (only a single chord was recorded). Although the signal-to-noise ratio for these data is high, their time resolution is poor (2 s). The data were reanalyzed by Elliot & Young (1991), who improved the accuracy of the radius limit and set upper limits on the column heights of any atmosphere. These limits range from 1 to 57 cm-am[1], depending on the gas. Elliot & Young (1991) noted hints that the immersion and emersion were not abrupt. If these effects are indeed due to a tenuous atmosphere, then the amount of gas needed to produce these effects range from 0.24 to 2.6 cm-am, again depending on the gas assumed to be present (0.39 ± 0.10 cm-am for CH_4). Additional data of higher time resolution and better quality will be needed to resolve the issue of a tenuous Charonian atmosphere with an Earth-based occultation. An ultraviolet solar-occultation observation from a spacecraft near Charon would be several orders of magnitude more sensitive a test for certain gases (depending on their cross sections for UV absorption).

CONCLUSIONS AND OPPORTUNITIES

In the period covered by this review, Earth-based stellar-occultation probes of planetary atmospheres have emerged from a curious, one-time-only opportunity to become an established technique that can be used regularly. Yet, before stellar occultations can reach their full potential, we need more high-quality data at more frequent intervals. Every last bit of signal-to-noise can tell us more about atmospheric structure, each additional chord adds to our knowledge about the spatial structure of an atmosphere, each new wavelength used opens new opportunities, and each new occultation event can reveal more about seasonal and climatic changes.

The promise of stellar-occultation investigations for the future may be best illustrated by Pluto and Triton, since one of the most fascinating aspects of these atmospheres are their (predicted) large, seasonal changes (Hansen & Paige 1992, Spencer & Moore 1992). This question could also be addressed with orbiting spacecraft, but these are unlikely for many decades. Despite the many similarities between Pluto and Triton—their sizes, densities, and main atmospheric constituent—their lower atmospheres exhibit quite different structures,

[1]cm-am refers to centimeter amagat, which is the equivalent amount of gas at STP in a column 1-cm high.

possibly due to a small difference in their CH_4 mixing ratios or the distribution of their N_2 surface ices. A fundamental question to answer for Triton is whether the atmospheric pressure is presently increasing or decreasing. Although large variations in Triton's surface pressure have been predicted, current uncertainties in the thermal inertia and N_2 inventory result in some models predicting an increase in surface pressure and others predicting a decrease. A series of stellar-occultation observations for Triton could establish the seasonal change of surface pressure, which could then be used to constrain the properties of Triton's surface ices. Another outstanding issue is to determine the nature of Pluto's lower atmosphere: Is there a haze layer or a thermal gradient or a combination of both causing the sharp drop in the occultation light curve (Figure 5)? A stellar occultation observed simultaneously in the visible and infrared would resolve this question. Also, a nearly central chord would probe more deeply than the KAO light curve and might detect a troposphere.

Considering analysis techniques, we have seen the shortcomings of both the model fitting and the inversion methods for learning the atmospheric structure. The upper region of a temperature profile derived from numerical inversion is sensitive to initial conditions, while the lower part of the profile is sensitive to the zero-flux calibration. Although model fitting is also sensitive to the zero-flux level, its main drawback is that you must know the correct form of the atmospheric model. So far these models have been limited to simple forms: isothermal, thermal gradient, extinction. However, as we become more skilled in constructing physical models for planetary atmospheres, we shall be able to extract more accurate information about atmospheric structure than we can presently obtain.

In the area of instrumentation, current detectors are well above 50% quantum efficiency, so we cannot expect much improvement in S/N from them. However, the larger collecting areas of telescopes being constructed will yield higher S/N and, even more importantly, will allow more frequent probing of atmospheres with occultations because fainter stars can be observed. These new, large telescopes will need high-speed array cameras suitable for occultation work.

The future also promises improvements in observing platforms. The KAO has proven to be an excellent platform for stellar occultations, primarily because it can be placed where needed to observe an event. The next-generation airborne observatory (SOFIA) will have a larger telescope aperture and a longer range. These factors will increase the number of high-S/N occultations available, especially for small-body occultations where the portability of the observatory is critical.

Finally, we note that one way to greatly increase the amount of planetary occultation data available in the future would be to launch a constellation of

three or more maneuverable, meter-class telescopes into large polar orbits. With this capability, the number of small-body events potentially observable would increase roughly as the radius of the orbit: about a factor of a hundred more events than we can access from the Earth for orbital radii equal to one-hundred Earth radii. More occultations by large planets would be observable too, with the added capability of getting chords widely spaced over the planet or multiple chords of the central flash. This type of facility would greatly enhance the usefulness of the stellar occultation technique for probing distant planetary atmospheres.

ACKNOWLEDGMENTS

We thank Bill Hubbard, Phil Nicholson, and Françoise Roques for supplying figures. Also, we appreciate comments on the manuscript from Bob Millis.

Literature Cited

Baron RL, French RG, Elliot JL. 1989. The oblateness of Uranus at the 1-μbar level. *Icarus* 78:119–30

Baum WA, Code AD. 1953. A photometric observation of the occultation of σ Arietis by Jupiter. *Astron. J.* 58:108–12

Born M, Wolf E. 1964. *Principles of Optics.* New York: Macmillan

Brinkmann RT. 1971. Occultation by Jupiter. *Nature* 230:515–16

Broadfoot AL, Atreya SK, Bertaux JL, Blamont JE, Dessler AJ, et al. 1989. Ultraviolet spectrometer observations of Neptune and Triton. *Science* 246:1459–66

Brouwer D, Clemence GM. 1961. Orbits and masses of planets and satellites. In *Planets and Satellites*, ed. GP Kuiper, BM Middlehurst, pp. 31–94. Chicago: Univ. Chicago Press

Buie MW, Tholen DJ, Horne K. 1992. Albedo maps of Pluto and Charon: Initial mutual event results. *Icarus* 97:221–27

Caldwell J, Cunningham CC, Anthony D, White HP, Groth EJ, et al. 1992. Titan: evidence for seasonal change—a comparison of Hubble Space Telescope and Voyager images. *Icarus* 97:1–9

Combes M, Lecacheux J, Vapillon L. 1971. First results of the occultation of β Sco by Jupiter. *Astron. Astrophys.* 15:235–38

Conrath B, Flasar FM, Hanel R, Kunde V, Maguire W, et al. 1989. Infrared observations of the Neptunian system. *Science* 246:1454–59

Conrath BJ, Gautier D, Hanel RA, Hornstein JS. 1984. The helium abundance of Saturn from Voyager measurements. *Astrophys. J.* 282:807–15

deVaucouleurs G, Menzel DH. 1960. Results of the occultation of Regulus by Venus, July 7, 1959. *Nature* 188:28–33

Dunham EW, McDonald SW, Elliot JL. 1991. Pluto-Charon stellar occultation candidates: 1990–1995. *Astron. J.* 102:1464–84

Elliot JL. 1979. Stellar occultation studies of the solar system. *Annu. Rev. Astron. Astrophys.* 17:445–75

Elliot JL, Baron RL, Dunham EW, French RG, Meech KJ, et al. 1985. The 1983 June 15 occultation by Neptune. I. Limits on a possible ring system. *Astron. J.* 90:2615–23

Elliot JL, Bosh AS, Cooke ML, Bless RC, Nelson MJ, et al. 1993. An occultation by Saturn's rings on 1991 October 2–3 observed with the Hubble Space Telescope. *Astron. J.* 106:2544–72

Elliot JL, Dunham E, Mink DJ, Churms J. 1980. The radius and ellipticity of Uranus from its

occultation of SAO 158687. *Astrophys. J.* 236:1026–30
Elliot JL, Dunham EW, Bosh AS, Slivan SM, Young LA, et al. 1989. Pluto's atmosphere. *Icarus* 77:148–70
Elliot JL, Dunham EW, Church C. 1976. A unique airborne observation. *Sky Telesc.* 52:23–25
Elliot JL, Dunham EW, Olkin CB. 1994. Exploring small bodies in the outer solar system with stellar occultations. In *Proc. Airborne Astronomy Symp. on the Galactic Ecosystem: From Gas to Stars to Dust*, ed. MR Haas, JA Davidson, EF Erickson, pp. 285–96. San Francisco: Astron. Soc. Pac.
Elliot JL, French RG, Dunham E, Gierasch PJ, Veverka J, et al. 1977a. Occultation of ϵ Geminorum by Mars. II. The structure and extinction of the Martian upper atmosphere. *Astrophys J.* 217:661-79
Elliot JL, French RG, Dunham E, Gierasch PJ, Veverka J, et al. 1977b. Occultation of ϵ Geminorum by Mars: Evidence for atmospheric tides? *Science* 195:485–86
Elliot JL, French RG, Frogel JA, Elias JH, Mink DJ, Liller W. 1981. Orbits of nine Uranian rings. *Astron. J.* 86:444–55
Elliot JL, Rages K, Veverka J. 1975a. The occultation of Beta Scorpii by Jupiter. VI. The masses of Beta Scorpii A_1 and A_2. *Astrophys. J. Lett.* 197:L123-26
Elliot JL, Veverka J. 1976. Stellar occultation spikes as probes of atmospheric structure and composition. *Icarus* 27:359–86
Elliot JL, Wasserman LH, Veverka J, Sagan C, Liller W. 1974. The occultation of Beta Scorpii by Jupiter. II. The hydrogen-helium abundance in the Jovian atmosphere. *Astrophys. J.* 190:719–29
Elliot JL, Wasserman LH, Veverka J, Sagan C, Liller W. 1975b. Occultation of β Scorpii by Jupiter. V. The emersion of β Scorpii C. *Astron. J.* 80:323–32
Elliot JL, Young LA. 1991. Limits on the radius and a possible atmosphere of Charon from its 1980 stellar occultation. *Icarus* 89:244–54
Elliot JL, Young LA. 1992. Analysis of stellar occultation data for planetary atmospheres. I. Model fitting, with application to Pluto. *Astron. J.* 103:991–1015
Eshleman VR. 1989. Pluto's atmosphere: Models based on refraction, inversion, and vapor-pressure equilibrium. *Icarus* 80:439–43
French RG, Elliot JL. 1979. Occultation of ϵ Geminorum by Mars. III. Temperature of the Martian upper atmosphere. *Astrophys. J.* 229:828–45
French RG, Elliot JL, Dunham EW, Allen DA, Elias JH, et al. 1983. The thermal structure and energy balance of the Uranian upper atmosphere. *Icarus* 53:399–414
French RG, Elliot JL, Gierasch PJ. 1978. Analysis of stellar occultation data. Effects of photon noise and initial conditions. *Icarus* 33:186–202
French RG, Elliot JL, Levine S. 1986. Structure of the Uranian rings. II. Ring orbits and widths. *Icarus* 67:134–63
French RG, Elliot JL, Sicardy B, Nicholson P, Matthews K. 1982. The upper atmosphere of Uranus: a critical test of isotropic turbulence models. *Icarus* 51:491–508
French RG, Lovelace RVE. 1983. Strong turbulence and atmospheric waves in stellar occultations. *Icarus* 56:122–46
French RG, Melroy PA, Baron RL, Dunham EW, Meech KJ, et al. 1985. The 1983 June 15 occultation by Neptune. II. The oblateness of Neptune. *Astron. J.* 90:2624–38
French RG, Nicholson PD, Cooke ML, Elliot JL, Matthews K, et al. 1993. Geometry of the Saturn system from the 3 July 1989 occultation of 28 Sgr and Voyager observations. *Icarus* 103:163–214
French RG, Taylor GE. 1981. Occultation of the ϵ Geminorum by Mars. IV. Oblateness of the Martian upper atmosphere. *Icarus* 45:577–85
Halliday I. 1965. A possible occultation by the planet Pluto. *Sky Telesc.* 29:216–17
Hansen CJ, Paige DA. 1992. A thermal model for the seasonal nitrogen cycle on Triton. *Icarus* 99:273–88
Harrington J, Cooke ML, Forrest WJ, Pipher JL, Dunham EW, Elliot JL. 1993. IRTF observations of the occultation of 28 Sgr by Saturn. *Icarus* 103:235–52
Hillier J, Veverka J. 1994. Photomeric properties of Triton hazes. *Icarus* 109:284–95
Hubbard WB. 1977. Wave optics of the central spot in planetary occultations. *Nature* 268:34–35
Hubbard WB. 1979. The ϵ Geminorum occultation: evidence for waves or turbulence. *Astrophys. J.* 229:821–27
Hubbard WB, Brahic A, Sicardy B, Elicer L-R, Roques F, Vilas F. 1986. Occultation detection of a neptunian ring-like arc. *Nature* 319:636–40
Hubbard WB, Haemmerle V, Porco CC, Rieke GH, Rieke MJ. 1995. The occultation of SAO 78505 by Jupiter. *Icarus* 113:103–9
Hubbard WB, Hunten DM, Dieters SW, Hill KM, Watson RD. 1988a. Occultation evidence for an atmosphere on Pluto. *Nature* 336:452–54
Hubbard WB, Hunten DM, Reitsema HJ, Brosch N, Nevo Y, et al. 1990a. Results for Titan's atmosphere from its occultation of 28 Sagittarii. *Nature* 343:353–55
Hubbard WB, Lellouch E, Sicardy B, Brahic

A, Vilas F, et al. 1988b. Structure of scintillations in Neptune's occultation shadow. *Astrophys. J.* 325:490–502

Hubbard WB, Nather RE, Evans DS, Tull RG, Wells DC, et al. 1972. The occultation of Beta Scorpii by Jupiter and Io. I. Jupiter. *Astron. J.* 77:41–59

Hubbard WB, Nicholson PD, Lellouch E, Sicardy B, Brahic A, et al. 1987. Oblateness, radius, and mean stratospheric temperature of Neptune from the 1985 August 20 occultation. *Icarus* 72:635–46

Hubbard WB, Porco CC, Hunten DM, Rieke GH, Rieke MJ, et al. 1993a. The occultation of 28 Sgr by Saturn: Saturn pole position and astrometry. *Icarus* 103:215–34

Hubbard WB, Sicardy B, Miles R, Hollis AJ, Forrest RW, et al. 1993b. The occultation of 28 Sgr by Titan. *Astron. Astrophys.* 269:541–63

Hubbard WB, Yelle RV, Lunine JI. 1990b. Nonisothermal Pluto atmosphere models. *Icarus* 84:1–11

Hunten DM, Veverka J. 1976. Stellar and spacecraft occultations by Jupiter: a critical review of derived temperature profiles. In *Jupiter,* ed. T Gehrels, pp. 247–83. Tucson: Univ. Ariz. Press

Jokipii JR, Hubbard WH. 1977. Stellar occultations by turbulent planetary atmospheres: the Beta Scorpii events. *Icarus* 30:537–50

Kovalevsky J, Link F. 1969. Diamètre aplatissement et propriétés optiques de la haute atmosphère de Neptune d'après l'occultation de l'étoile BD-17° 4388. *Astron. Astrophys.* 2:398–412

Lellouch E. 1994. Pluto's atmospheric structure: clear vs hazy models. *Icarus* 108:225–64

Lellouch E, Hubbard WB, Sicardy B, Vilas F, Bouchet P. 1986. Occultation determination of Neptune's oblateness and stratospheric methane mixing ratio. *Nature* 324:227–31

Lindal GF, Lyons JR, Sweetnam DN, Eshleman VR, Hinson DP, Tyler GL. 1987. The atmosphere of Uranus: results of radio occultation measurements with *Voyager 2. J. Geophys. Res.* 92:14,987–5001

Lindal GF, Wood GE, Hotz HB, Sweetnam DN, Eshleman VR, Tyler GL. 1983. The atmosphere of Titan: an analysis of the *Voyager 1* radio occultation measurements. *Icarus* 53:348–63

McDonald SW, Elliot JL. 1995. Triton stellar occultation candidates: 1995–1999. *Astron. J.* 109:1352–62

Millis RL, Wasserman LH, Franz OG, Nye RA, Elliot JL, et al. 1993. Pluto's radius and atmosphere: results from the entire 9 June 1988 occultation data set. *Icarus* 105:282–97

Narayan R, Hubbard WB. 1988. Theory of anisotropic refractive scintillation: application to stellar occultations by Neptune. *Astrophys. J.* 325:503–18

Nicholson PD, McGhee C, French RG. 1995. Saturn's central flash from the 3 July 1989 occultation of 28 Sgr. *Icarus* 113:57–83

Olkin CB, Elliot JL. 1994. Occultation astrometry: predictions and post-event results. In *Galactic and Solar System Optical Astrometry,* ed. LV Morrison, GF Gilmore, pp. 286–90. Cambridge: Cambridge Univ. Press

Olkin CB, Elliot JL, Bus SJ, McDonald SW, Dahn CC. 1996. Astrometry of single-chord occultations: application to the 1993 triton event. *Publ. Astron. Soc. Pac.* 108:202–10

Owen T, Biemann K, Rushneck DR, Biller JE, Howarth DW, Lafleur AL. 1977. The composition of the atmosphere at the surface of Mars. *J. Geophys. Res.* 82:4635–39

Owen TC, Roush TL, Cruikshank DP, Elliot JL, Young LA, et al. 1993. Surface ices and the atmospheric composition of Pluto. *Science* 261:745–78

Pannekoek A. 1904. Über die Erscheinungen, welche bei einer Sternbadeckung durch einer Planeten auftreten. *Astron. Nach.* 164:5–10

Roques F, Sicardy B, French RG, Hubbard WB, Barucci A, et al. 1994. Neptune's upper stratosphere, 1983–1990: ground-based stellar occultation observations. *Astron. Astrophys.* 288:985–1011

Seiff A, Kirk DB. 1977. Structure of Mars' atmosphere up to 100 kilometers from the entry measurements of Viking 2. *Science* 194:1300–3

Sicardy B, Brahic A, Ferrari C, Gautier D, Lecacheux J, et al. 1990. Probing Titan's atmosphere by stellar occultation. *Nature* 343:350–53

Smith BA, Soderblom LA, Banfield D, Barnet C, Basilevksy AT, et al. 1989. *Voyager 2* at Neptune: imaging science results. *Science* 246:1422–49

Smith GR, Hunten DM. 1990. Study of planetary atmospheres by absorptive occultations. *Rev. Geophys.* 28:117–43

Smith GR, Strobel DF, Broadfoot AL, Sandel BR, Shemansky DE, Holberg JB. 1982. Titan's upper atmosphere: composition and temperature from the EUV solar occultation results. *J. Geophys. Res.* 87:1351–59

Spencer JR, Moore JM. 1992. The influence of thermal inertia on temperatures and frost stability on Triton. *Icarus* 99:261–72

Stansberry JA, Lunine JI, Hubbard WB, Yelle RV, Hunten DM. 1994. Mirages and the nature of Pluto's atmosphere. *Icarus* 111:503–13

Stern SA, Trafton L. 1984. Constraints on bulk composition, seasonal variation, and global

dynamics of Pluto's atmosphere. *Icarus* 57:231–40
Strobel DF, Zhu X, Summers ME, Stevens MH. 1995. On the vertical thermal structure of Pluto's atmosphere. *Icarus* In press
Taylor GE. 1963. The occultation of Regulus by Venus on 1959 July 7. *R. Obs. Bull.* E355–E66
Texas-Arizona Occultation Group. 1977. The occultation of epsilon Geminorum by Mars: analysis of McDonald data. *Astrophys. J.* 214:934–45
Toon OB, McKay CP, Griffith CA, Turco RP. 1992. A physical model of Titan's aerosols. *Icarus* 95:24–54
Trafton L. 1990. A two-component volatile atmosphere for Pluto. I. The bulk hydrodynamic escape regime. *Astrophys. J.* 359:512–23
Tryka KM, Brown RH, Cruikshank DP, Owen TC, Geballe TR, DeBergh C. 1994. The temperature of nitrogen ice on Pluto and its implications for flux measurements. *Icarus* 112:513–27
Tyler GL, Eshleman VR, Anderson JD, Levy GS, Lindal GF, et al. 1982. Radio science with *Voyager 2* at Saturn: atmosphere and ionosphere and the masses of Mimas, Tethys, and Iapetus. *Science* 215:553–58
Tyler GL, Sweetnam DN, Anderson JD, Borutzki SE, Campbell JK, et al. 1989. Voyager radio science observations of Neptune and Triton. *Science* 246:1466–73
Vapillon L, Combes M, Lecacheux J. 1973. The β Scorpii occultation by Jupiter. II. The temperature and density profiles of the Jovian upper atmosphere. *Astron. Astrophys.* 29:135–49
Veverka J, Wasserman L. 1974. The Regulus occultation light curve and the real atmosphere of Venus. *Icarus* 21:196–98
Veverka J, Wasserman LH, Elliot J, Sagan C, Liller W. 1974. The occultation of β Scorpii by Jupiter. I. The structure of the Jovian upper atmosphere. *Astron. J.* 79:73–84
Walker AR. 1980. An occultation by Charon. *MNRAS* 192:P47–50
Warwick JW, Evans DR, Romig JH, Sawyer CB, Desch MD, et al. 1986. *Voyager 2* radio observations of Uranus. *Science* 233:102–6
Wasserman LH, Millis RL, Williamon RM. 1977. Analysis of the occultation of ϵ Geminorum by Mars. *Astron. J.* 82:506–10
Wasserman LH, Veverka J. 1973a. Analysis of spikes in occultation curves: a critique of Brinkmann's method. *Icarus* 18:599–604
Wasserman LH, Veverka J. 1973b. On the reduction of occultation light curves. *Icarus* 20:322–45
Yelle RV, Lunine JI. 1989. Evidence for a molecule heavier than methane in the atmosphere of Pluto. *Nature* 339:288–90
Yelle RV, Lunine JI, Hunten DM. 1991. Energy balance and plume dynamics in Triton's lower atmosphere. *Icarus* 89:347–58
Young AT. 1976. Scintillations during occultations by planets. I. An approximate theory. *Icarus* 27:335–57
Young EF, Binzel RP. 1994. A new determination of radii and limb parameters for Pluto and Charon from mutual event lightcurves. *Icarus* 108:219–24
Zurek RW. 1974. *Tides in the Martian atmosphere.* PhD thesis. Univ. Wash., Seattle
Zurek RW. 1976. Diurnal tide in the Martian atmosphere. *J. Atmos. Sci.* 33:321–37